



## Noble metal nanoparticles modified ZnS quantum dots as visible light photocatalysts for wastewater treatment

Nader Sherif<sup>1</sup>, Yasser Abdelmonem<sup>1\*</sup>, Farag A. Ali<sup>1</sup>, Tarek A. Gad-Allah<sup>2</sup>  
and Metwally Madkour<sup>3\*\*</sup>

<sup>1</sup> Chemistry Department, Faculty of Science, Menoufia University, 32511, Shebin El-Kom, Egypt.

<sup>2</sup> Department of Water Pollution Control, Environmental Science Division, National Research Centre

<sup>3</sup> Chemistry Department, Faculty of Science, Kuwait University, P.O. Box 5969, Safat 13060, Kuwait.

\*Corresponding author, Email address: [ykabelmonem@gmail.com](mailto:ykabelmonem@gmail.com)

\*\*Corresponding author, Email address: [metwally.madkour@ku.edu.kw](mailto:metwally.madkour@ku.edu.kw)

Received 06 Mar 2022,  
Revised 22 Mar 2022,  
Accepted 26 Mar 2022

### Keywords

- ✓ Quantum dots
- ✓ Noble metals,
- ✓ Photocatalysis,
- ✓ Nanoparticles,

\*Corresponding author,  
Email address:

[ykabelmonem@gmail.com](mailto:ykabelmonem@gmail.com)

\*\*Corresponding author,  
Email address:

[metwally.madkour@ku.edu.kw](mailto:metwally.madkour@ku.edu.kw)

### Abstract

Semiconductor quantum dots (QDs) are fascinating materials due to their optoelectronic applications. Nanoparticle semiconductors that have been doped with noble metals like platinum and palladium are referred to as plasmonic photocatalysts. Despite the fact that several groups have reported the fabrication of ZnS QDs, only a few have found ways to synthesize noble metal doped ZnS QDs. We investigated a gram-scale, environmentally friendly, room-temperature, aqueous solution-based approach to the synthesis of renewable and environmentally friendly materials, highly distributed undoped ZnS quantum dots as well as noble metal doped ZnS QDs in this research (loading amount 4 wt). XRD, XPS, and TEM methods were utilized to determine the characteristics of the nanophotocatalysts. The ZnS QDs have been observed to have modest diameters of around 4.5 nm and an optical band gap,  $E_g$ , of 3.86 eV which is reduced upon the introduction of noble metals and reached 2.6. The photocatalytic activity of non-doped and doped ZnS QDs was tested using methylene blue photodegradation. Doping ZnS QDs with Pd and Pt nanoparticles leads in a considerable improvement in the photocatalytic efficiency. because of the magnitude of the noble metals' Schottky barrier, which prevents charge carrier recombination and, as a result, The photogenerated electrons' lifetime is extended.

## 1. Introduction

Pollutants in industrial wastewater are a major source of concern for the environment. Dyes found in wastewater from the textile, paper, and plastics industries are particularly hazardous in this regard. Importantly, around 15% of dyes used in industrial processes are lost [1, 2]. They represent a major threat to living beings since many of the dyes are poisonous and carcinogenic [3]. As a result, there is a pressing need to discover innovative technologies for removing hazardous dyes from wastewater.

Heterogeneous photocatalyzed reactions are widely regarded as one of the most promising strategies for removing organic contaminants from water in natural settings [4, 5]. II-VI semiconductors have been the most thoroughly investigated photocatalysts used for this purpose due to their unique physical features and widespread availability [6]. When a semiconductor is photoexcited, an electron goes into the conduction band while a hole (positive charge) is created in the valence band. Charge carriers, which are produced from positive holes and negative conduction band electrons, could oxidize, and reduce a variety of organic molecules adsorbed on the semiconductor surface. These mechanisms cause the

chemicals to mineralize by converting them to CO<sub>2</sub>, H<sub>2</sub>O, and mineral acids [7] under ideal circumstances. However, because quick recombination of an electron and a hole leads in non-productive deactivation of the photocatalyst's excited state, the efficiency of these redox processes are limited [8].

It is widely assumed that using noble metals to modify the surface of a semiconductor improves photocatalytic efficiency [9]. The efficiency improvements are the result of several mechanisms that are influenced by operational conditions. Noble metals can prevent electron/hole recombination by acting as electron traps, hence extending the lifetimes of charge carriers. Furthermore, these metals can cause light absorbed by semiconductors to extend into the visible range due to a surface plasmon resonance phenomenon. Finally, noble metal coatings can be used to change the surface characteristics of semiconductors [10-13]. ZnS doped with noble metals has crucial environmental applications as photocatalysts in wastewater treatment operations [14-16]. Many studies on the effects of doping ZnS with Mn, Cu, or Ni have been published [17, 18]. Only a few research on the effects of doping ZnS with Pd and Pt nanoparticles, on the other hand, have been conducted.

Although there are numerous papers on the synthesis of ZnS quantum dots, only a few concerns have been raised about the facile preparation of ZnS QDs and/or the development of one-step, aqueous, room temperature synthetic procedures [19]. The aim of this study is investigating a facile method to prepare solar active photocatalysts based on binary chalcogenide (ZnS) by doping with noble metals such as platinum and palladium. Therefore, we established a simple, one-pot approach for the manufacture of monodispersed undoped and noble metal doped ZnS QDs using a PVP/PVA polymer blend as the growth media in the study detailed below. In terms of band structure, the nanoparticles' optoelectronic capabilities were determined. The photocatalytic capabilities of the produced nanoparticles were evaluated utilizing methylene blue photodegradation. Finally, a simple washing technique was created for reactivating the photocatalyst.

## **2. Methodology**

### **2.1. Preparation of ZnS QDs.**

In a typical QD synthesis, 0.2 M Zinc nitrate is added to a 100 mL of 5% aqueous solution of PVP/PVA (50/50 wt %) with stirring. Then an equal volume of a 0.2 M aqueous solution of Na<sub>2</sub>S as the sulfur source is added and the resulting solution is allowed to stir till obtaining homogeneity. This mixture is transferred to a 300 mL Teflon lined stainless-steel autoclave and let stand at 110 °C for 5 h. Centrifugation gives a precipitate that is washed several times with doubly distilled water and ethanol. The final white precipitate of ZnS QDs is dried overnight at 70 °C.

### **2.2. Preparation of Pd,Pt/ZnS QDs.**

The solution of protecting agent (Pd,Pt/PVA=1.5:1 mg mg<sup>-1</sup>) is added to palladium sulfate or potassium tetra chloroplatinate (10mg/100ml) at room temperature under stirring to 10 min in order to prepare Pd/ZnS QDs and Pt/ZnS QDs, respectively. An aqueous solution of sodium borohydride (Pd,Pt/NaBH<sub>4</sub>=2.5:5.0 mol mol<sup>-1</sup>) is then added under stirring for 30 min, then ZnS QDs was added to the solution to have finally a noble metal loading of 4 wt.%. The stirring was continued for further 180 min. Finally, an extensive washing by de-ionized water was carried out for 4 times with a consecutive separation of the powder by centrifugation at 12000 rpm for 30 min. The resulting powder was dried in oven at 90 °C.

### **2.3. Characterization of the prepared nanoparticles**

The bulk and surface characterization of the prepared nanoparticles were investigated by X-ray Powder diffraction (XRD) measurements were carried on a Bruker, D8 ADVANCE diffractometer using Cu K $\alpha$

( $\lambda = 0.154$  nm) radiation under 40 kV, 40 mA with scanning in the range of 20–80° 2 $\theta$ . Morphological characterization was conducted by transmission electron microscopy (TEM) using a JEOL JEM 1230 (JEOL Ltd., Japan) operating at 120 KV. Surface elemental analysis by X-ray photoelectron spectroscopy (XPS) was measured on a VG ESCALAB2 XPS spectrometer with an Al K $\alpha$  monochromatic source and a charge neutralizer. All binding energies are referenced to C 1s peak at 284.5 eV. Optical properties of the samples were studied by UV–Vis spectroscopy using Varian Cary 5000 UV.

#### 2.4. Photocatalytic measurements

The photocatalytic efficiencies of non-doped and noble metal doped ZnS QDs (50 ppm) were assessed by using photodegradation of methylene blue (MB, 5 ppm) in an aqueous solution (100 mL) at room temperature using solar irradiation. MB solutions (pH 6.2) containing suspended QDs were first magnetically stirred in the dark for 0.5 h to achieve homogeneity. The intensity of natural sun irradiation was measured between February 15 and March 03, 2022, on days when there were no clouds, and the sky was clear in Shebin El-Kom (30°33'31"N 31°00'36"E). The incoming sun energy was measured to be about 79.100 flux (625 W/m<sup>2</sup>) employing a digital illumination meter (INS, DX-200). At fixed time intervals, irradiation was terminated, and 3 mL aliquots of the suspensions were removed, centrifuged and analyzed to determine MB concentrations by using UV–Vis spectroscopy. Following immediate return of the aliquots to the reaction container irradiation was begun.

### 3. Results and Discussion

#### 3.1 Characterization of nanoparticles

XRD pattern of ZnS QDs spectra show various diffraction peaks at 2 $\theta$  values of 29.33, 48.80 and 57.61 corresponding to the diffraction planes (111), (220) and (311), respectively (Figure 1) [20]. The average crystalline size was obtained as 3.5 nm using Debye–Scherrer equation [21].

For Pd/ZnS and Pt/ZnS, the diffraction peaks displayed a slight shift to lower 2 $\theta$  values indicates lattice compression because of the larger ionic radius of Pd ( 1.37 Å) and Pt ( 1.39 Å) than that of Zn<sup>2+</sup> ( 0.74 Å), confirming the integration of the noble metals in the prepared ZnS lattice [22, 23]. The crystallite sizes were calculated from the full width at half-maximum of the (200) peak profile at the value of 2 $\theta$  = 27.4° for ZnS using the Scherrer equation:

$$d(\text{Å}) = K\lambda / \beta \cos \theta \quad (1)$$

Where  $d$  is the average crystallite size and the number  $K = 0.9$  is a coefficient,  $\lambda = 0.1541$  nm is the X-Ray wavelength,  $\beta$  is the full width half maximum (FWHM) of the catalyst,  $\theta$  is the diffracting angle. The average crystallite size of the ZnS NPs, Pd/ZnS and Pt/ZnS were calculated, and the results were found to be 3.4, 4.2 and 4.6 for ZnS NPs, Pd/ZnS and Pt/ZnS respectively. The crystallite size data revealed the increase in size after doping of ZnS with Pd and Pt which is another proof for the successful incorporation of Pd and Pt within ZnS lattice [24].

The size and morphologies of produced nanoparticles were studied using the TEM. It depicts the bare ZnS and noble metal doped ZnS QDs, which were assembled in a cluster, as having a homogeneous spherical shape structure. It demonstrates that the surface has a lot of homogeneity. The particles have a ball-like shape that is approximately spherical. Figure 2 shows TEM pictures of prepared ZnS QDs with individual particles in the 4.5–5.5 nm range, confirming the XRD data. The high-resolution XPS spectra for the Pt 4f, Pd 3d, Zn 2p, and S 2p binding energy regions are shown in Fig. 2. The binding energies of Zn 2p<sub>1/2</sub> and 2p<sub>3/2</sub> of the prepared sample of ZnS and observed at 1045.0 and 1022.1 eV respectively.

The spin-orbit splitting of Zn  $2p_{3/2}$  and Zn  $2p_{1/2}$  is 23.0 eV, which is characteristic for ZnS [25]. The S  $2p_{1/2}$ , the binding energy is observed at 162.0 eV which is in accordance with previously reported work [26].

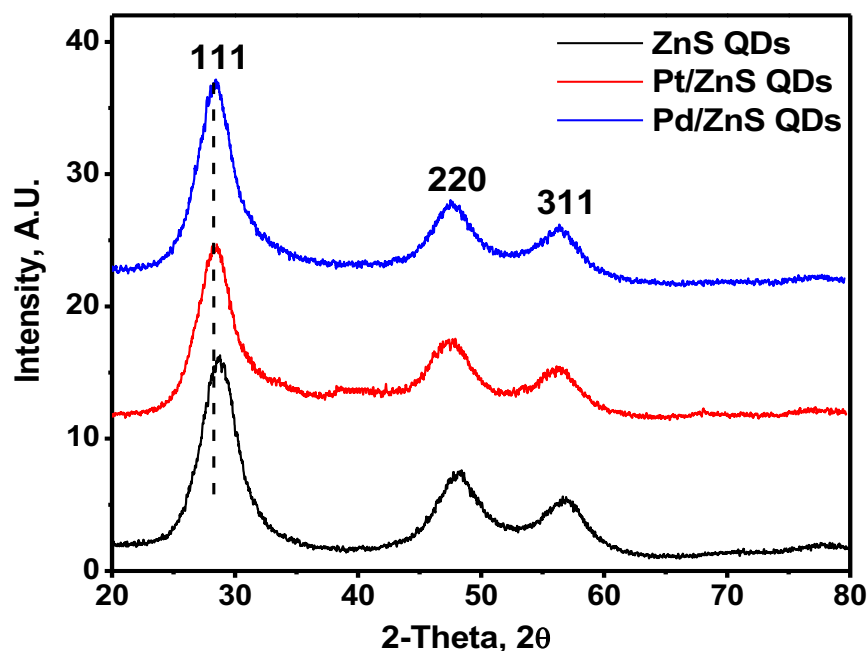


**Fig. 1** XRD patterns of ZnS, Pd/ZnS and Pt/ZnS nanoparticles

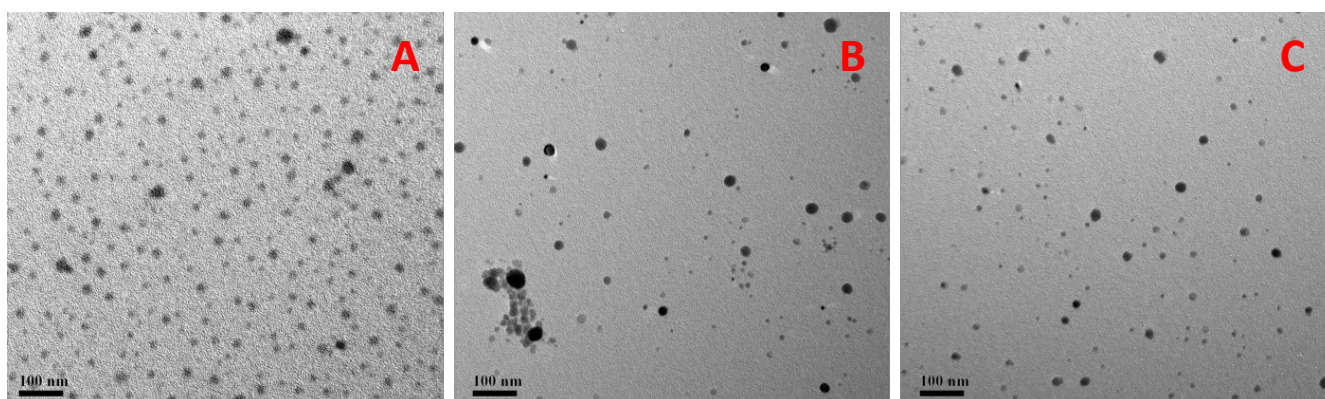


**Fig. 2** TEM images of (A) ZnS, (B) Pd/ZnS and (C) Pt/ZnS nanoparticles

In sample Pt/ZnS, the high-resolution Pt 4f spectrum shown in Figure 3 confirmed the presence of single metallic state of Pt. The peaks in Fig. 3 appeared at 74.4 eV and 71.1 eV are corresponding to the Pt  $4f_{5/2}$  and Pt  $4f_{7/2}$ , respectively which are assigned to be metallic state (Pt $^0$ ) [27]. In sample Pd/ZnS, the high resolution Pd 3d spectrum shown in Figure 3 confirmed the presence of single metallic state of Pd. The doublets corresponding to Pd  $3d_{5/2}$  and Pd  $3d_{3/2}$  states that locate around (335.41 and 340.68 eV) and (336.03 and 340.94 eV) were attributed to metallic Pd $^0$  [28]. Also, the splitting energy between Pd  $3d_{3/2}$  and Pd  $3d_{5/2}$  as shown in Figure 3 is 5.27 eV, which proved the presence of metallic Pd [29]. Figure 4 reveals the absorption spectra of the prepared nanoparticles. From the figure it is revealed that non-doped ZnS nanoparticles do not absorb light in the visible region and have an absorption beginning at 315 nm. The doped equivalents Pt/ZnS and Pd/ZnS, on the other hand, absorb light far into the visual range. Using this data, the band gap energies ( $E_g$ ) of undoped and doped ZnS QDs were calculated. The calculated band gap energy of undoped ZnS QDs was found to be 3.93 eV, while those for the respective Pt/ZnS and Pd/ZnS are blue shifted to 2.31 and 2.67.

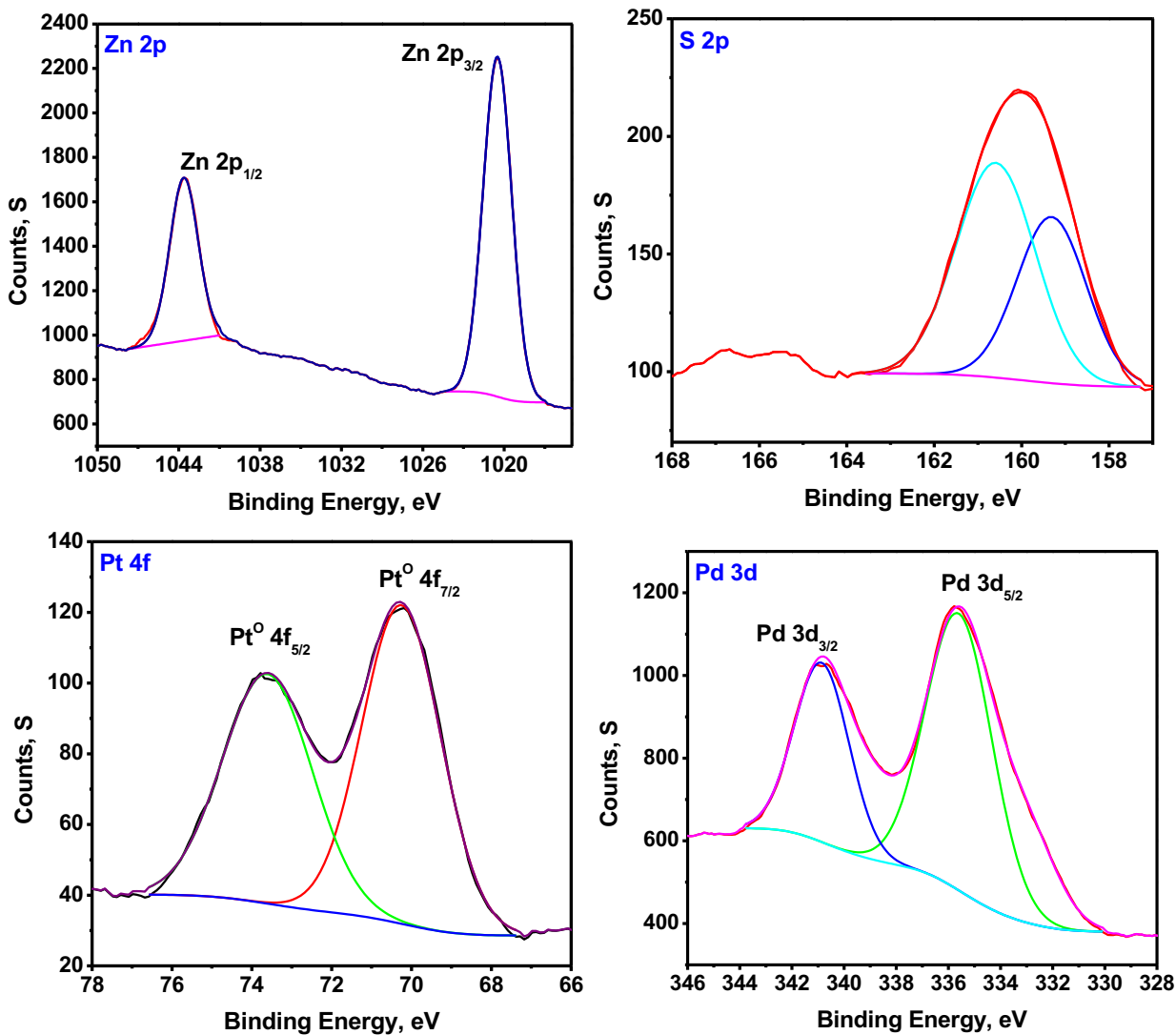


**Fig. 3:** Deconvoluted XPS spectra of Zn2p, S2p, Pt 4f and Pd 3d in ZnS, Pd/ZnS and Pt/ZnS nanoparticles

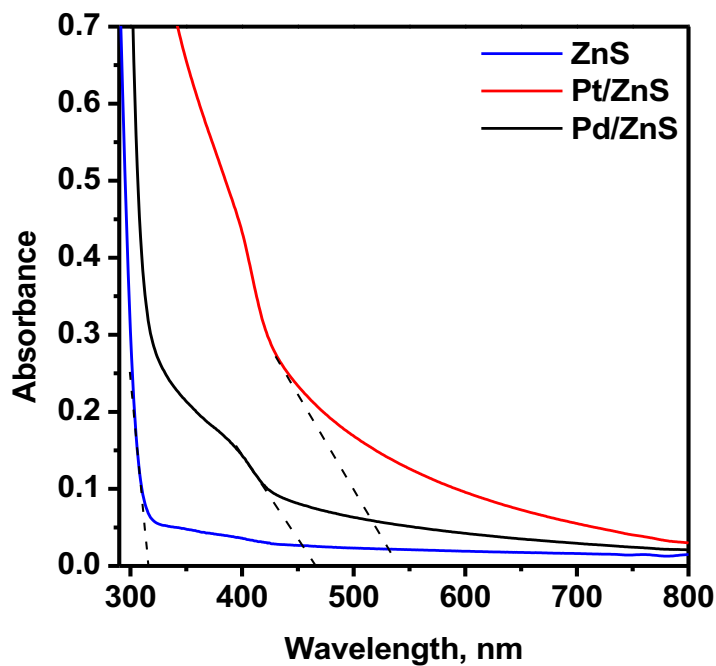


**Fig. 4:** UV-Vis spectra for ZnS, Pd/ZnS and Pt/ZnS nanoparticles

### 3.2. Photocatalytic degradation efficiency

Electron transfer between the catalyst and the pollutant promotes redox and subsequent chemical reactions in one pathway for photocatalyzed degradation of organic pollutants. The light used in this process must have an energy that is consistent with the photocatalyst's optical band gap [30]. However, the efficiency of the photocatalyst-promoted degradation process is not solely determined by its band gap configuration. Another important factor is the photogenerated electron's transit and lifetime, which are influenced by the conduction and valence band locations [31]. The photodegradation process follows a pseudo-first-order rate profile under continuous irradiation, which may be stated as  $\ln(C_0/C) = kt$ , where  $C_0$  and  $C$  are the pollutant's starting concentration and concentration at time  $t$ , respectively, and  $k$  is the apparent first-order rate constant. As a result, a plot of  $\ln C_0/C$  vs time should be linear, with the slope providing the apparent first-order rate constant  $k$ . Figure 5 shows the rates and efficiencies for methylene blue photodegradation reactions catalyzed by different photocatalysts.

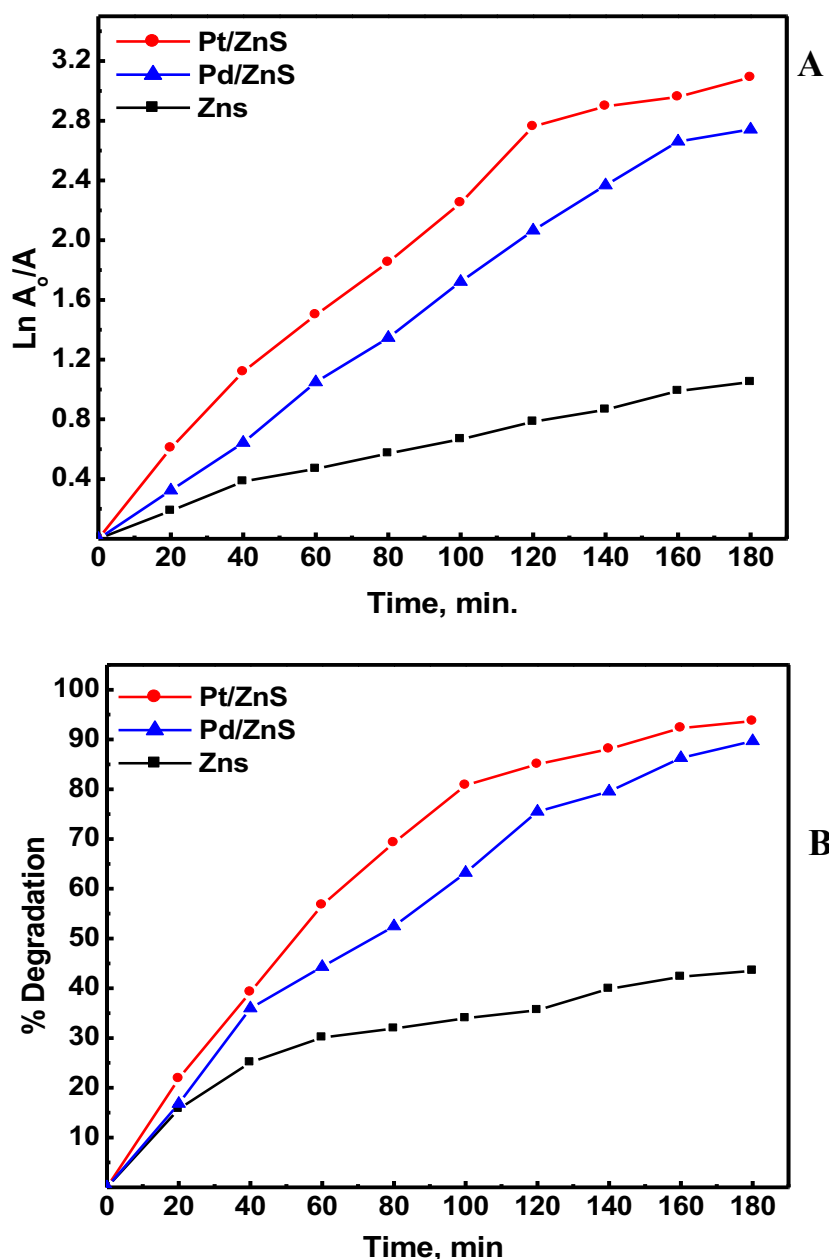


**Figure 5:** Plots of (A)  $\ln C_0/C$  vs. time. and (B) degradation efficiency for MB removal by the prepared materials.

As shown in Figure 5, the photodegradation rate obtained in case of doped ZnS NPs was calculated and found to be very high as they revealed photodegradation rates of  $14.4 \times 10^{-3}$  and  $17.3 \times 10^{-3} \text{ min}^{-1}$  for Pd/ZnS and Pt/ZnS, respectively compared with  $7.3 \times 10^{-3} \text{ min}^{-1}$  for bare ZnS.

The findings show that decreasing the band gap of the nano photocatalyst reduces the effectiveness of the MB photodegradation process by allowing for easier electron/hole recombination in the excited state of the catalyst. Because of their reduced electron/hole recombination rates, Pd and Pt NPs were found to have higher photocatalytic efficiencies than non-doped ZnS [32]. The Fermi values of Pd and Pt NPs are lower than those of ZnS. As a result, photo-excited electrons can be transported to the surface conduction bands of Pd and Pt in doped ZnS QDs. Photo-generated valence band holes, on the other hand, remain on ZnS, resulting in a charge separation that reduces the likelihood of electron-hole recombination and improves photocatalytic effectiveness [33-35].

P-type semiconductor band energies bend upwards (or downwards) in the direction of metal dopant band energy to a degree that is depending on their relative work functions. The transfer of electrons between the semiconductor and the metal at the contact causes band bending [36, 37]. The work functions of the noble metals, Pd and Pt, and the band structure of pure ZnS can be compared using a potential scale that is relative to the standard hydrogen electrode (NHE). Because multiple factors (such as loading amount) were employed, it has not been able to establish which noble metals metal dopant leads to the best photocatalyst performance so far [38]. We believe that the Fermi level energy of the noble metal used as dopant will correlate with photocatalytic efficiencies. Considering the electrochemical reduction potentials for Pt and Pd [ $E^{\circ}_{\text{reduction}}(\text{Pt}^{2+} + 2e^{-} \rightarrow \text{Pt}) = 1.2 \text{ V}$  and  $E^{\circ}_{\text{reduction}}(\text{Pd}^{2+} + 2e^{-} \rightarrow \text{Pd}) = 0.83 \text{ V}$ ], it can be seen that the reduction potential of Pt is closer to the valence band of ZnS. As a result, the MB degradation reaction photocatalyzed by Pt/ZnS should be the most efficient [39], a prediction that matches the experimental results.

### 3.3. Repeatability and reactivation of nanophotocatalysts.

The consistency of MB photodegradation processes induced by undoped and noble metal doped ZnS QDs was investigated. Following each reaction cycle, the photocatalyst was collected, washed with doubly distilled water, and dried before being reused in this investigation. The experimentally determined MB degradation efficiencies across five cycles (Figure not shown) reveal that photocatalyst deactivation happens continuously when the catalysts are reused, as expected.

After the fifth cycle, the photocatalysts were reactivated by washing with a dilute acetic acid solution and then an alkaline solution. The final pH value was always set to be higher than the isoelectric point. The washing technique is carried out for two reasons. The first step is to eliminate excess hydroxide ions, which inhibit the photocatalyst's active sites and prevent dye adsorption. The second step is to make the surface sufficiently anionic so that the dye can be attracted to it electrostatically [40]. The results reveal that washing the ZnS QDs regenerates all of their photocatalytic activity for Pt/ZnS had 90.6 % regenerated activity, respectively (5th cycle,).

## Conclusion

In this study, we developed a new approach for producing well dispersed undoped ZnS QDs as well as Pt and Pd doped ZnS QDs on a large scale in an environmentally friendly manner in this study. The photocatalytic properties of non-doped and doped ZnS QDs were evaluated by using them to enhance methylene blue photodegradation. The results show that when noble metal nanoparticles are doped, photodegradation efficiency has improved. The improved photocatalytic activities of noble metal doped ZnS QDs can be explained in terms of the Schottky barrier of noble metals, which limits charge carrier

recombination and so extends the lifetime of photogenerated electrons. The fact that Pt/ZnS is more active than Pd/ZnS in catalyzing the photodegradation of MB supports this conclusion. Finally, a study was conducted to see if the photocatalysts could be regenerated so that they may be used in the long run. The results suggest that by eliminating the hydroxide ion, simple washing methods can be employed to revive the catalysts. The overall result of this research is that while creating an optimal nanophotocatalyst, both optoelectronic qualities and isoelectric point must be considered.

**Disclosure statement:** *Conflict of Interest:* The authors declare that there are no conflicts of interest. *Compliance with Ethical Standards:* This article does not contain any studies involving human or animal subjects.

## References

- [1] A. Khataee, M.B. Kasiri, Photocatalytic degradation of organic dyes in the presence of nanostructured titanium dioxide: Influence of the chemical structure of dyes, *Journal of Molecular Catalysis A: Chemical*, 328 (2010) 8-26.
- [2] N. Daneshvar, M. Rabbani, N. Modirshahla, M. Behnajady, Critical effect of hydrogen peroxide concentration in photochemical oxidative degradation of CI Acid Red 27 (AR27), *Chemosphere*, 56 (2004) 895-900.
- [3] J. Kiwi, C. Pulgarin, P. Peringer, M. Grätzel, Beneficial effects of homogeneous photo-Fenton pretreatment upon the biodegradation of anthraquinone sulfonate in waste water treatment, *Applied Catalysis B: Environmental*, 3 (1993) 85-99.
- [4] J.-M. Herrmann, Photocatalysis fundamentals revisited to avoid several misconceptions, *Applied Catalysis B: Environmental*, 99 (2010) 461-468.
- [5] M. Pelaez, N.T. Nolan, S.C. Pillai, M.K. Seery, P. Falaras, A.G. Kontos, P.S. Dunlop, J.W. Hamilton, J.A. Byrne, K. O'shea, A review on the visible light active titanium dioxide photocatalysts for environmental applications, *Applied Catalysis B: Environmental*, 125 (2012) 331-349.
- [6] E. Pelizzetti, Concluding remarks on heterogeneous solar photocatalysis, *Solar energy materials and solar cells*, 38 (1995) 453-457.
- [7] M. Salaices, B. Serrano, H. De Lasa, Photocatalytic conversion of phenolic compounds in slurry reactors, *Chemical Engineering Science*, 59 (2004) 3-15.
- [8] F.M. Pesci, G. Wang, D.R. Klug, Y. Li, A.J. Cowan, Efficient Suppression of Electron-Hole Recombination in Oxygen-Deficient Hydrogen-Treated TiO<sub>2</sub> Nanowires for Photoelectrochemical Water Splitting, *J Phys Chem C Nanomater Interfaces*, 117 (2013) 25837-25844 DOI: [10.1021/jp4099914](https://doi.org/10.1021/jp4099914).
- [9] C. Han, M.-Q. Yang, N. Zhang, Y.-J. Xu, Enhancing the visible light photocatalytic performance of ternary CdS-(graphene-Pd) nanocomposites via a facile interfacial mediator and co-catalyst strategy, *Journal of Materials Chemistry A*, 2 (2014) 19156-19166.
- [10] J. Jiang, H. Li, L. Zhang, New insight into daylight photocatalysis of AgBr@ Ag: synergistic effect between semiconductor photocatalysis and plasmonic photocatalysis, *Chemistry—A European Journal*, 18 (2012) 6360-6369.
- [11] S. Shen, L. Guo, X. Chen, F. Ren, C.X. Kronawitter, S.S. Mao, Effect of noble metal in CdS/M/TiO<sub>2</sub> for photocatalytic degradation of methylene blue under visible light, *International Journal of Green Nanotechnology: Materials Science & Engineering*, 1 (2010) M94-M104.
- [12] S. Liu, Z. Qu, X. Han, C. Sun, A mechanism for enhanced photocatalytic activity of silver-loaded titanium dioxide, *Catalysis Today*, 93 (2004) 877-884.
- [13] M. Jakob, H. Levanon, P.V. Kamat, Charge distribution between UV-irradiated TiO<sub>2</sub> and gold nanoparticles: determination of shift in the Fermi level, *Nano letters*, 3 (2003) 353-358.

- [14] X. Jin, F. Chen, D. Jia, Y. Cao, H. Duan, M. Long, Facile strategy for the fabrication of noble metal/ZnS composites with enhanced photocatalytic activities, *RSC Advances*, 10 (2020) 4455-4463 DOI: [10.1039/C9RA07163F](https://doi.org/10.1039/C9RA07163F).
- [15] M. Madkour, F. Al Sagheer, Au/ZnS and Ag/ZnS nanoheterostructures as regenerated nanophotocatalysts for photocatalytic degradation of organic dyes, *Optical Materials Express*, 7 (2017) 158-169 DOI: [10.1364/OME.7.000158](https://doi.org/10.1364/OME.7.000158).
- [16] P. Sivakumar, G.K. Gaurav Kumar, P. Sivakumar, S. Renganathan, Synthesis and characterization of ZnS-Ag nanoballs and its application in photocatalytic dye degradation under visible light, *Journal of Nanostructure in Chemistry*, 4 (2014) 107 DOI: [10.1007/s40097-014-0107-0](https://doi.org/10.1007/s40097-014-0107-0).
- [17] A. Zaba, S. Sovinska, T. Kirish, A. Wegrzynowicz, K. Matras-Postolek, Photodegradation Process of Organic Dyes in the Presence of a Manganese-Doped Zinc Sulfide Nanowire Photocatalyst, *Materials (Basel, Switzerland)*, 14 (2021) 5840 DOI: [10.3390/ma14195840](https://doi.org/10.3390/ma14195840).
- [18] X. Liu, Y. Zhang, S. Matsushima, T. Sugiyama, H. Hojo, H. Einaga, Rational Design of Cu-Doped ZnS Nanospheres for Photocatalytic Evolution of H<sub>2</sub> with Visible Light, *ACS Applied Energy Materials*, 5 (2022) 1849-1857 DOI: [10.1021/acsaem.1c03323](https://doi.org/10.1021/acsaem.1c03323).
- [19] F. Al-Sagheer, A. Bumajdad, M. Madkour, B. Ghazal, Optoelectronic characteristics of ZnS quantum dots: simulation and experimental investigations, *Science of Advanced Materials*, 7 (2015) 2352-2360.
- [20] D.W. Synnott, M.K. Seery, S.J. Hinder, G. Michlits, S.C. Pillai, Anti-bacterial activity of indoor-light activated photocatalysts, *Applied Catalysis B: Environmental*, 130 (2013) 106-111.
- [21] X. Li, F. Wang, Q. Qian, X. Liu, L. Xiao, Q. Chen, Ag/TiO<sub>2</sub> nanofibers heterostructure with enhanced photocatalytic activity for parathion, *Materials Letters*, 66 (2012) 370-373.
- [22] D. Chen, T. Li, Q. Chen, J. Gao, B. Fan, J. Li, X. Li, R. Zhang, J. Sun, L. Gao, Hierarchically plasmonic photocatalysts of Ag/AgCl nanocrystals coupled with single-crystalline WO<sub>3</sub> nanoplates, *Nanoscale*, 4 (2012) 5431-5439 DOI: [10.1039/c2nr31030a](https://doi.org/10.1039/c2nr31030a).
- [23] R. Chimentao, I. Kirm, F. Medina, X. Rodriguez, Y. Cesteros, P. Salagre, J. Sueiras, J. Fierro, Sensitivity of styrene oxidation reaction to the catalyst structure of silver nanoparticles, *Applied surface science*, 252 (2005) 793-800.
- [24] C. Xu, Y. Liu, B. Huang, H. Li, X. Qin, X. Zhang, Y. Dai, Preparation, characterization, and photocatalytic properties of silver carbonate, *Applied surface science*, 257 (2011) 8732-8736.
- [25] N. Maheshwari, L. Tatikondewar, S. KULKARNI, S. Acharya, A. Kshirsagar, Ethylenediamine-Mediated Wurtzite Phase Formation in ZnS, (2013).
- [26] M.H. Ullah, I. Kim, C.-S. Ha, pH selective synthesis of ZnS nanocrystals and their growth and photoluminescence, *Materials Letters*, 61 (2007) 4267-4271.
- [27] Q. Shi, C. Zhu, M.H. Engelhard, D. Du, Y. Lin, Highly uniform distribution of Pt nanoparticles on N-doped hollow carbon spheres with enhanced durability for oxygen reduction reaction, *RSC advances*, 7 (2017) 6303-6308.
- [28] L.J. Wang, J. Zhang, X. Zhao, L.L. Xu, Z.Y. Lyu, M. Lai, W. Chen, Palladium nanoparticle functionalized graphene nanosheets for Li-O<sub>2</sub> batteries: enhanced performance by tailoring the morphology of the discharge product, *RSC advances*, 5 (2015) 73451-73456.
- [29] N. Chen, D. Deng, Y. Li, X. Liu, X. Xing, X. Xiao, Y. Wang, TiO<sub>2</sub> nanoparticles functionalized by Pd nanoparticles for gas-sensing application with enhanced butane response performances, *Sci Rep*, 7 (2017) 7692 DOI: [10.1038/s41598-017-08074-y](https://doi.org/10.1038/s41598-017-08074-y).
- [30] H. Wang, L. Zhang, Z. Chen, J. Hu, S. Li, Z. Wang, J. Liu, X. Wang, Semiconductor heterojunction photocatalysts: design, construction, and photocatalytic performances, *Chem Soc Rev*, 43 (2014) 5234-5244 DOI: [10.1039/c4cs00126e](https://doi.org/10.1039/c4cs00126e).
- [31] L. Kong, Z. Jiang, H.H.-C. Lai, T. Xiao, P.P. Edwards, Does noble metal modification improve the photocatalytic activity of BiOCl?, *Progress in Natural Science: Materials International*, 23 (2013) 286-293.

- [32] J. Colmenares, M. Aramendia, A. Marinas, J. Marinas, F. Urbano, Synthesis, characterization and photocatalytic activity of different metal-doped titania systems, *Applied Catalysis A: General*, 306 (2006) 120-127.
- [33] R. Sonawane, M. Dongare, Sol-gel synthesis of Au/TiO<sub>2</sub> thin films for photocatalytic degradation of phenol in sunlight, *Journal of Molecular Catalysis A: Chemical*, 243 (2006) 68-76.
- [34] M. Valden, X. Lai, D.W. Goodman, Onset of catalytic activity of gold clusters on titania with the appearance of nonmetallic properties, *science*, 281 (1998) 1647-1650 DOI: [10.1126/science.281.5383.1647](https://doi.org/10.1126/science.281.5383.1647).
- [35] V. Vamathevan, R. Amal, D. Beydoun, G. Low, S. McEvoy, Photocatalytic oxidation of organics in water using pure and silver-modified titanium dioxide particles, *Journal of Photochemistry and Photobiology A: Chemistry*, 148 (2002) 233-245.
- [36] J.-M. Herrmann, H. Tahiri, Y. Ait-Ichou, G. Lassaletta, A. Gonzalez-Elipse, A. Fernandez, Characterization and photocatalytic activity in aqueous medium of TiO<sub>2</sub> and Ag-TiO<sub>2</sub> coatings on quartz, *Applied Catalysis B: Environmental*, 13 (1997) 219-228.
- [37] V. Subramanian, E.E. Wolf, P.V. Kamat, Catalysis with TiO<sub>2</sub>/gold nanocomposites. Effect of metal particle size on the Fermi level equilibration, *J Am Chem Soc*, 126 (2004) 4943-4950 DOI: [10.1021/ja0315199](https://doi.org/10.1021/ja0315199).
- [38] A. Bumajdad, M. Madkour, Understanding the superior photocatalytic activity of noble metals modified titania under UV and visible light irradiation, *Phys Chem Chem Phys*, 16 (2014) 7146-7158 DOI: [10.1039/c3cp54411g](https://doi.org/10.1039/c3cp54411g).
- [39] Y.-Y. Hsu, N.-T. Suen, C.-C. Chang, S.-F. Hung, C.-L. Chen, T.-S. Chan, C.-L. Dong, C.-C. Chan, S.-Y. Chen, H.M. Chen, Heterojunction of Zinc Blende/Wurtzite in Zn<sub>1-x</sub> Cd<sub>x</sub> S Solid Solution for Efficient Solar Hydrogen Generation: X-ray Absorption/Diffraction Approaches, *ACS applied materials & interfaces*, 7 (2015) 22558-22569.
- [40] D. Chen, F. Huang, G. Ren, D. Li, M. Zheng, Y. Wang, Z. Lin, ZnS nano-architectures: photocatalysis, deactivation and regeneration, *Nanoscale*, 2 (2010) 2062-2064 DOI: [10.1039/c0nr00171f](https://doi.org/10.1039/c0nr00171f).

(2022) ; <http://www.jmaterenvironsci.com>